Implementation and Comparison of SiC and GaN switches for EV Fast Recharging Systems

Daniele Scirè
Department of Engineering
University of Palermo
Palermo, Italy
daniele.scire@unipa.it

Giovanni Garraffa
Faculty of Engineering and Architecture
University of Enna Kore
Enna, Italy
giovanni.garraffa@unikore.it

Giuseppe Lullo
Department of Engineering
University of Palermo
Palermo, Italy
giuseppe.lullo@unipa.it

Gianpaolo Vitale
Institute for High Performance Computer and Networking
National Research Council of Italy
Palermo, Italy
gianpaolo.vitale@icar.cnr.it

Pasquale Cusumano
Department of Engineering
University of Palermo
Palermo, Italy
pasquale.cusumano@unipa.it

Michele Calabretta
ADG Power and Discretes R&D Division
STMicroelectronics
Catania, Italy
michele.calabretta@st.com

Angelo Alberto Messina
R&D and Public Affairs
STMicroelectronics
Catania, Italy
angelo.messina@st.com

Giuseppe Costantino Giaconia
Department of Engineering
University of Palermo
Palermo, Italy
costantino.giaconia@unipa.it

Alessandro Busacca
Department of Engineering
University of Palermo
Palermo, Italy
alessandro.busacca@unipa.it

Antonino Sferlazza
Department of Engineering
University of Palermo
Palermo, Italy
antonino.sferlazza@unipa.it

***Abstract*—. Wide bandgap material-based devices allow faster switching frequency and exhibit smaller losses than traditional Si devices; nevertheless, a complete understanding of the functioning of these new devices remains poorly understood. A fast battery charger for electric vehicles based on a converter employing SiC and GaN devices is here reported Besides, these two technologies are experimentally compared, in the same layout, to highlights their performance in terms of electrical dynamic and electromagnetic compatibility.**

Keywords—DC-DC converter, SiC, GaN, isolated converter, EMI

I. Introduction

The development of power electronics systems and applications, demanding high power and high-frequency operations, settled attention in development of novel semiconductor materials [1], [2]. Indeed, silicon faces formidable competition from Silicon Carbide (SiC) and Gallium Nitride (GaN); these wide-bandgap materials offer significant advantages over traditional silicon-based switches [1].

The silicon carbide presents a wider bandgap than silicon, making it capable of withstanding higher voltages and temperatures. This property alone has profound implications for power electronics, as it allows for developing devices that can operate at higher power levels while maintaining efficiency [3]. Furthermore, the high electron mobility of SiC enables faster switching speeds, reducing switching losses and improving overall system efficiency. This property is precious in applications where high-frequency operation is essential, such as electric vehicles (EVs) and renewable energy systems [4], [5]. Additionally, SiC devices exhibit lower on-resistance, resulting in reduced conduction losses, a critical factor in high-power applications. The ability of SiC devices to withstand elevated temperatures without significant degradation in performance is another compelling feature. The thermal robustness of SiC devices allows for compact designs with minimal cooling requirements, contributing to the miniaturization of power electronic systems [6].

The advantages of SiC are reflected in its diverse range of applications. SiC diodes and MOSFETs are increasingly used in high-frequency converters, providing remarkable gains in efficiency. In EVs, SiC-based inverters offer higher power density, extending the driving range while reducing charging times. SiC is also instrumental in enabling grid-tied solar inverters and power supplies with enhanced efficiency and reliability. Moreover, SiC's resilience to high-temperature operation finds applications in aerospace and defense, where electronic systems often operate in extreme environments. The ability to reduce the size and weight of power electronics while improving performance is a game-changer in these sectors. The maximum junction temperature of SiC exceeds 600 °C but is mainly limited by bonding and packaging techniques; therefore, the commercial devices reach a maximum temperature of 210 °C [7].

Gallium Nitride (GaN) is another wide-bandgap material that has gained traction in power electronics. GaN devices, like SiC, offer exceptional material properties such as high electron mobility, allowing for fast switching and reduced switching losses [8]. GaN's ability to operate efficiently at high frequencies makes it ideal for applications such as wireless power transfer, RF amplifiers, and high-frequency converters. Furthermore, GaN devices can be manufactured on smaller wafers than SiC, making them cost-competitive for specific applications; moreover, GaN's integration into silicon-based technology is straightforward, facilitating its adoption in existing electronic systems. While GaN offers remarkable advantages, it is not without challenges. GaN devices are more susceptible to damage from voltage spikes, necessitating careful circuit design and protection mechanisms [9].

Both SiC and GaN switches have strengths and limitations. SiC excels in high-temperature and high-voltage applications, making it well-suited for EVs, renewable energy, and aerospace. GaN, conversely, shines in high-frequency and compact designs, making it suitable for telecommunications,

This work was realized into the project frame of REACTION "first and euRopEAn siC eighT Inches pilOt liNe", co-funded by the ECSEL Joint Undertaking under grant agreement No 783158 [10]

979-8-3503-8106-1/23/$31.00 ©2023 IEEE

consumer electronics, and automotive applications. The choice between SiC and GaN depends on the application's specific requirements. Engineers must consider voltage and current ratings, switching frequency, thermal management, and cost constraints when selecting the appropriate semiconductor material.

The objective of this paper is to make a comparative analysis of the electrical performances of an electronic system designed for fast recharging of batteries for EVs. To this aim, they are implemented on the same board layout. As the market share for eco-friendly alternatives to traditional combustion engines rises, there is a strong demand for efficient and high-power charging solutions. Such solutions include stations capable of delivering high power levels to reduce charging times through high-voltage compact DC converters, on-board chargers that connect directly to the AC grid to achieve faster charging times than the standard stations, and even wireless charging for an enhanced user experience. In this context, using power electronic switches capable of offering superior performance compared to traditional silicon-based switches is essential. SiC and GaN provide higher switching frequencies with reduced losses, improving the overall system efficiency, maintaining a compact size, tolerating high-temperature operations, and achieving a reduced cooling need. Conversely, the accessibility of wide bandgap material-based devices remains constrained, and the understanding of the functioning of these devices is not yet fully developed leading to numerous challenges in the field of reliability and electromagnetic compatibility.

This paper aims to test and compare the functioning of these devices when implemented in dedicated EV fast recharging of batteries system based on an isolated DC-DC converter. To properly compare the performance, including near field high frequencies, a suitable PCB has been designed. Two identical boards have been realized equipped with the GaN and SiC devices. The MOSFET switches will implement GaN and SiC devices to compare the system's electrical performance and evaluate the radiated power inside a semi-anechoic chamber. The results will give a better insight and understanding of the use of these switches based on wide-bandgap materials.

II. Experimental Details

A. The isolated DC-DC converter

Figure 1 depicts a simple schematization of the realized isolated DC-DC converter. The circuit rely on a high-frequency transformer to achieve the galvanic insulation. The converter is composed by an inverter implementing wide-bandgap material MOSFETs, a transformer and a rectifier which use SiC diodes. The switches *Q1-Q4* compose the full bridge, *T* is the transformer, *D1-D4* are the SiC diodes of the rectifier, *C* is the output capacitor, and R_L the load resistor. A digital signal processor is used to produce the driving command for the MOSFETs resulting in two pulse-width-modulation commands shifted by an angle of 180°. The two signals share the same duty cycle *D* which vary in the rage 0-1. When the duty cycle is <1/2, the circuit operates in buck mode, otherwise in boost mode. Table I reports: MOSFETs, diodes, and driver. The transformer T is a planar transformer whose specifications are in Table II.

TABLE I. Main Components

Component	Value
SiC MOSFETs	SCTWA90N65G2V
GaN MOSFETs	GAN041-650WSBQ
Diodes	STPSC40H12C
MOSFET driver	STGAP2SCIC

TABLE II. Transformer Specifications

Specific	Value
Max output power	12 kW
Operating frequency	100-200 kHz
Primary inductance	2 mH ±25%
Turn ratio primary to secondary	13:2

B. PCB of the switching circuit

The guidelines provided in the STGAP2SICS datasheet [11] were used to develop the printed circuit board. Figure 2 illustrates the Miller Clamp and negative gate driving schematic. The Miller clamp function enables the regulation of the Miller current during the switching in half-bridge configurations. When the external power transistor is in the OFF state, the driver operates to prevent the potential induced turn-on that may occur when the other switch of the same leg is being turned on.

Throughout the turn-off period, the CLAMP pin monitors the gate of the external switch. The CLAMP switch is activated when the gate voltage exceeds the voltage threshold, establishing a low-impedance path between the switch gate and the GNDISO pin. Figure 3 shows the implemented boards, while the test-rig, situated in the semi-anechoic chamber, encompassed various elements of the test-rig is presented in Fig. 4. Finally, the high voltage DC-link power supply is shown in Fig. 5. The Table III reports the employed instrumentation and control system.

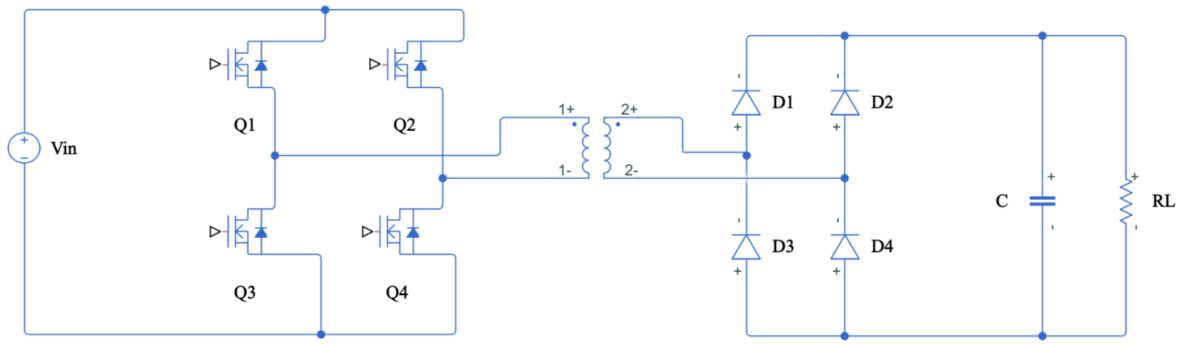

Fig. 1. Isolated DC-DC converter schematic

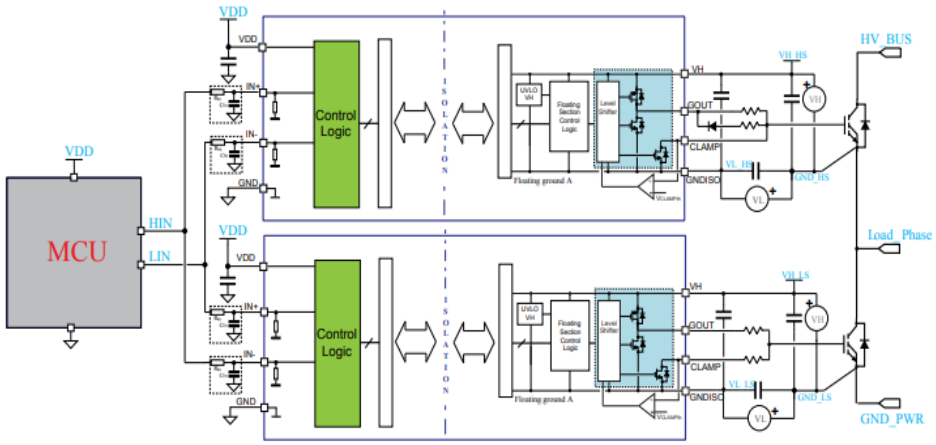

Fig. 2 Miller Clamp and negative gate driving application diagram [11].

Fig. 3 Two boards implementing the halft bridge converters.

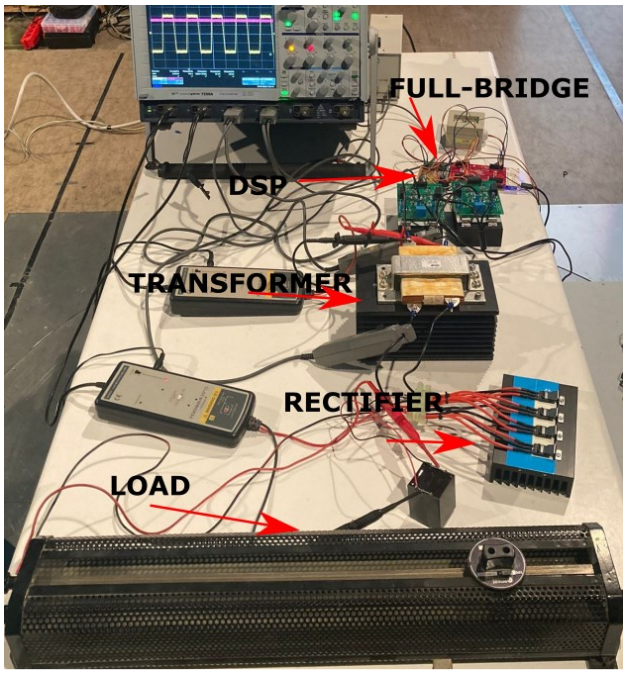

Fig. 4. The test-rig assembled in the semi-anechoic chamber.

Fig. 5. DC-link high-voltage power supply.

TABLE III. TEST RIG INSTRUMENTATION

Element	Value
DC-link power supply	MagnaPower LXI 1000 V 30 A
Control DC power supply	5 V power bank
Control board	LAUNCHXL-F28379D
Load	200 Ω - 1 kW rheostat

The feedback system applies the timing logic, described in Section II.A, and the feedback system, allowing the control of the converter output.

A double voltage and current loop control the isolated full-bridge converter. PI (Proportional-Integral) controllers represent both the voltage and the current regulators. The cut-off frequency of the open loop system is lower than the converter switching frequency; therefore, the PWM converter is modeled as proportional considering the transformer turns ratio N. Furthermore, since the cut-off frequency of the inner loop is higher than the external voltage loop, the adjusting of the PI controllers result in a simple and easy procedure.

III. Results

The experimental results highlight the proper functioning of the DC-DC converter considering 800 W power transfer. The input voltage is 500 V, and the switching frequency is 100 kHz. The converter produces an output DC voltage of 400 V. Two identical sets of boards were realized, each implementing a half bridge configuration: a couple equipped with SiC devices and a second couple with GaN devices. Except for this, the boards are identical. Experimental results prove the correct functioning of the converter employing the SiC devices and the GaN devices.

A. Transient analysis

Figure 6 shows the voltage-waveform at the output of the full-bridge, which is the square wave produced by switching SiC MOSFETs. The transient is analyzed in better detail in Fig. 7, where the timescale is expanded, highlighting a slope of 1250 V/μs and an oscillation of 10 MHz.

Similarly, Fig. 8 voltage-waveform at the output of the full-bridge equipped with the GaN MOSFETs; the transient is analyzed in better detail in Fig. 9, where the timescale is expanded, highlighting similar results to the SiC case with a slope of 1250 V/μs and a 10 MHz oscillation.

In Fig. 10, the comparison of the first part of the slope is depicted for both the case implementing SiC and GaN MOSFETs; it shows that during the first 40 ns after the switch command, there is a different slope in the rising voltage of the two converters with the converter implementing the GaN switches showing a faster slope.

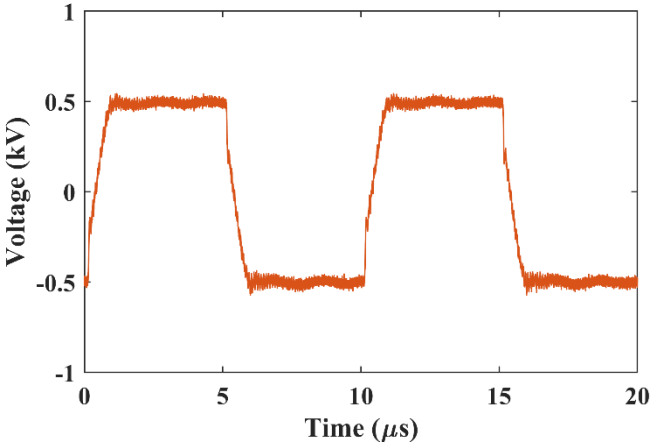

Fig. 6. Primary side voltage for the converter implementing the SiC MOSFETs.

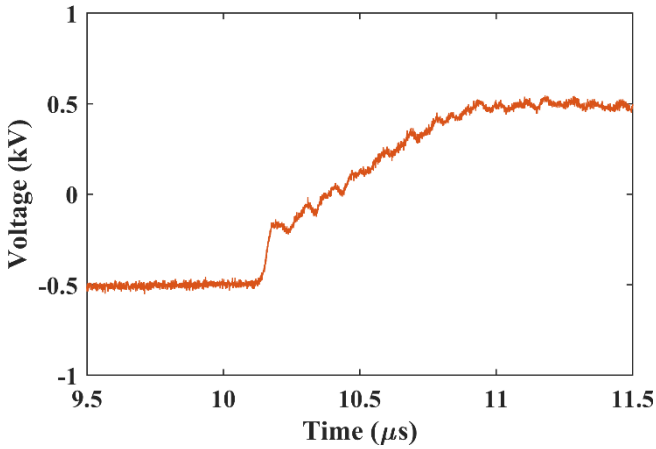

Fig. 7. Expanded time scale of the primary side for the converter implementing the SiC MOSFETs.

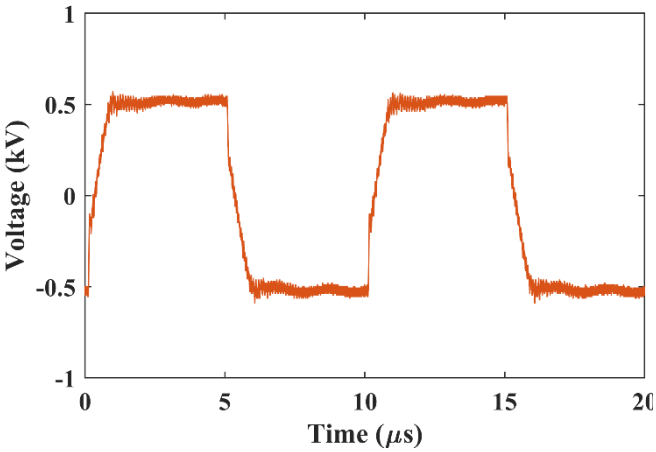

Fig. 8. Primary side voltage for the converter implementing the GaN MOSFETs.

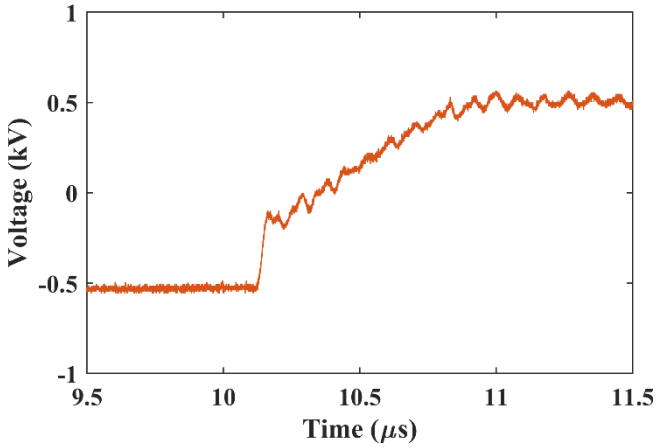

Fig. 9. Expanded time scale of the primary side voltage for the converter implementing the GaN MOSFETs.

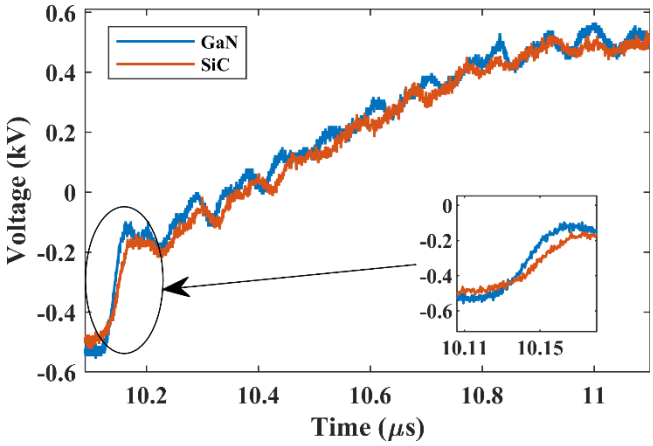

Fig. 10. Expanded time scale comparison of the primary side voltage for the converter implementing the GaN and SiC MOSFETs.

B. *Near field analysis*

An electromagnetic interference analysis has been carried out to evaluate the difference in behavior between the converter implementing the SiC devices and the GaN devices. It should be noted that the board layout using the GaN device and SiC MOSFETs are identical, and only the switches were changed. A simple copper coil placed in close contact with the MOSFET was used to couple the radiated field induced by the switching operations; the oscilloscope probe was then connected to the terminations of the coil to visualize the signal. The distance of the coil from the MOSFETs was identical for all the measurements. Figure 11 shows the coupled signal for the board implementing the SiC devices, whereas an expanded time scale is shown in Fig. 12. The switching of the MOSFETs causes the ringing in the signal with a frequency of 15 MHz. Figure 13 shows the coupled signal for the board implementing the GaN devices, whereas an expanded time scale is shown in Fig. 14, showing a frequency of the pseudo-oscillation of 15 MHz with an amplitude almost twice as compared to the signal coupled to the board implementing the SiC switches.

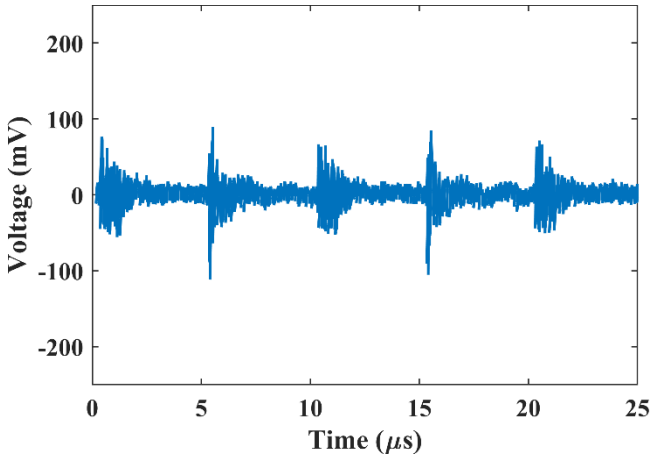

Fig. 11. Coupled signal from the converter implementing the SiC MOSFETs.

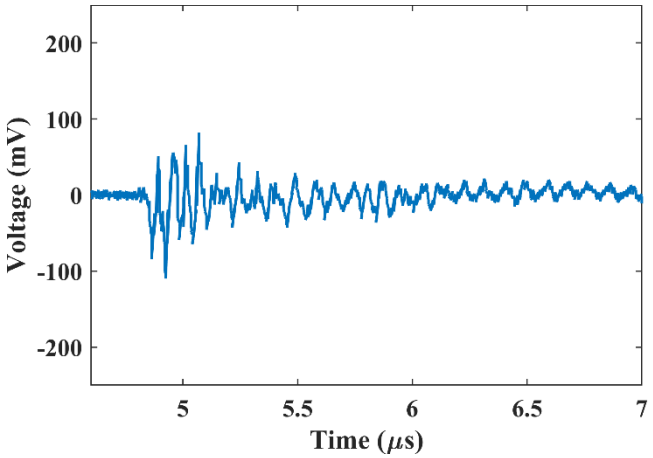

Fig. 12. Expanded time scale of the coupled signal from the converter implementing the SiC MOSFETs.

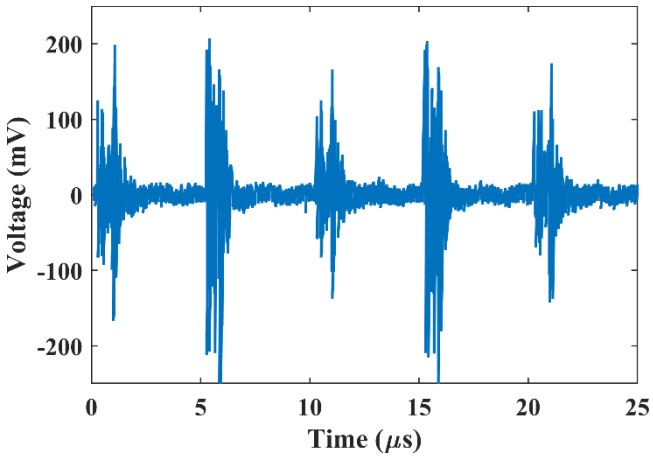

Fig. 13. Coupled signal from the converter implementing the GaN MOSFETs.

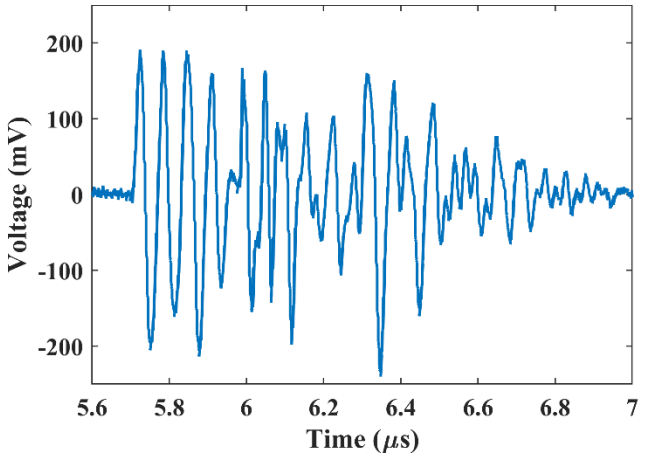

Fig. 14. Expanded time scale of the coupled signal from the converter implementing the GaN MOSFETs.

IV. Conclusions

A DC-DC converter designed for automotive application implementing SiC and GaN devices is reported to study the behavior of these wide bandgap device. Two identical converters were realized: one with SiC MOSFETs and one with GaN devices. A set of experimental tests, here reported, evaluated the performance of the converter. The output voltage shown a reduced ripple due to the high frequency of the PWM signal. The effect of the different devices was analyzed through the measurements of the near field, showing

that the use of GaN based switches generates harmonics with higher amplitude in the near field, mainly due to the faster rising voltage. As all other components and the PCB where identical, this difference in EMI is due only to the switching characteristics of the power devices. It is interesting that a small increase of the speed of the rising voltage results on a relevant near field harmonic content. A broad study of the electromagnetic compatibility should be performed when using high-bandgap devices.

REFERENCES

[1] H. Lee, V. Smet, and R. Tummala, "A Review of SiC Power Module Packaging Technologies: Challenges, Advances, and Emerging Issues," *IEEE J Emerg Sel Top Power Electron*, vol. 8, no. 1, pp. 239–255, Mar. 2020, doi: 10.1109/JESTPE.2019.2951801.

[2] D. J. Perreault *et al.*, "Opportunities and Challenges in Very High Frequency Power Conversion," in *2009 Twenty-Fourth Annual IEEE Applied Power Electronics Conference and Exposition*, IEEE, Feb. 2009, pp. 1–14. doi: 10.1109/APEC.2009.4802625.

[3] X. She, A. Q. Huang, O. Lucia, and B. Ozpineci, "Review of Silicon Carbide Power Devices and Their Applications," *IEEE Transactions on Industrial Electronics*, vol. 64, no. 10, pp. 8193–8205, Oct. 2017, doi: 10.1109/TIE.2017.2652401.

[4] F. Pellitteri *et al.*, "Power losses comparison between Silicon Carbide and Silicon devices for an isolated DC-DC converter," in *2021 IEEE 15th International Conference on Compatibility, Power Electronics and Power Engineering (CPE-POWERENG)*, IEEE, Jul. 2021, pp. 1–6. doi: 10.1109/CPE-POWERENG50821.2021.9501191.

[5] D. Scire, G. Lullo, and G. Vitale, "Design and modeling of an interleaving boost converter with quasi-saturated inductors for electric vehicles," in *2020 AEIT International Conference of Electrical and Electronic Technologies for Automotive, AEIT AUTOMOTIVE 2020*, Torino, Italy: IEEE, Nov. 2020, pp. 1–6. doi: 10.23919/aeitautomotive50086.2020.9307424.

[6] J. Wang and X. Jiang, "Review and analysis of SiC MOSFETs' ruggedness and reliability," *IET Power Electronics*, vol. 13, no. 3, pp. 445–455, Feb. 2020, doi: 10.1049/iet-pel.2019.0587.

[7] X. Guo, Q. Xun, Z. Li, and S. Du, "Silicon Carbide Converters and MEMS Devices for High-temperature Power Electronics: A Critical Review," *Micromachines (Basel)*, vol. 10, no. 6, p. 406, Jun. 2019, doi: 10.3390/mi10060406.

[8] J. Gareau, R. Hou, and A. Emadi, "Review of Loss Distribution, Analysis, and Measurement Techniques for GaN HEMTs," *IEEE Trans Power Electron*, vol. 35, no. 7, pp. 7405–7418, Jul. 2020, doi: 10.1109/TPEL.2019.2954819.

[9] N. Keshmiri, D. Wang, B. Agrawal, R. Hou, and A. Emadi, "Current Status and Future Trends of GaN HEMTs in Electrified Transportation," *IEEE Access*, vol. 8, pp. 70553–70571, 2020, doi: 10.1109/ACCESS.2020.2986972.

[10] A. A. Messina *et al.*, "The 'first and euRopEAn siC eighT Inches pilOt liNe': A project, called REACTION, that will boost key SiC Technologies upgrading (developments) in Europe, unleashing Applications in the Automotive Power Electronics Sector," in *2020 AEIT International Conference of Electrical and Electronic Technologies for Automotive, AEIT AUTOMOTIVE 2020*, 2020. doi: 10.23919/aeitautomotive50086.2020.9307385.

[11] STmicroelectronics, "STGAP2SICS Datasheet." Accessed: Sep. 14, 2023. [Online]. Available: https://www.st.com/resource/en/datasheet/stgap2sics.pdf